



Effect of cooling rate on microstructural evolution and hardness of self-shielded arc weld deposits containing 1 wt% aluminium

M. Dumovic^{1,2} · D. Dunne² · J. Norrish² · H. Li² · B. J. Monaghan²

Received: 7 November 2016 / Accepted: 6 February 2018 / Published online: 20 February 2018
© International Institute of Welding 2018

Abstract

The self-shielded arc welding is based on the presence of flux elements that protect the weld from oxygen and nitrogen. The hardfacing alloy investigated contained about 1 wt% Al to prevent weld porosity by combining with oxygen and nitrogen. Thermodynamic calculations of the phase equilibria for the alloy predicted a weld metal microstructure consisting of δ -ferrite and austenite at high temperatures. Since the alloy had a high hardenability, the austenite transformed to martensite on cooling to provide a hardfacing deposit microstructure that is resistant to metal-to-metal wear. Nevertheless, the high Al content ensured that δ -ferrite was present as the minor microstructural component in all of weld deposits examined. The cooling rate after welding is a key variable that influences the volume fractions of δ -ferrite and martensite in the weld deposit. Dilatometric studies reported in this paper show that increasing the cooling rate of samples subjected to a weld thermal cycle designed to simulate the effect of pre-heat resulted in increases in volume percentage martensite, the magnitude of the transformation volume change and the M_S temperature. Using a pre-heat temperature higher than M_S resulted in the isothermal formation of bainite, as well as martensite on subsequent cooling. Despite the multiphase microstructure of bainite, martensite and δ -ferrite, the weldment hardness was considerably more uniform than for deposits produced using lower temperature, conventional, pre-heats. In general, deposition at the higher temperature served the purpose of normalising the hardness by reducing differences in dislocation density and carbide precipitation throughout the various regions of the weld deposit.

Keywords Hardfacing · Wear · Heat affected zone · Phase transformations · Microstructures

Recommended for publication by Commission II - Arc Welding and Filler Metals

✉ M. Dumovic
milo.dumovic@solidtechnologies.com.au

D. Dunne
druce@uow.edu.au

J. Norrish
johnn@uow.edu.au

H. Li
huijun@uow.edu.au

B. J. Monaghan
monaghan@uow.edu.au

¹ Solid Technologies Pty. Ltd./University of Wollongong, Wollongong, Australia

² Australia, Faculty of Engineering and Information Sciences, School of Mechanical, Materials and Mechatronic Engineering, University of Wollongong, Wollongong, Australia

1 Introduction

The benefits of weld hardfacing for repair and maintenance have been well established through comprehensive research and practical applications [1, 2].

Tubular self-shielded flux cored wires without shielding gas protection have been successfully applied to a large variety of welding applications including surfacing and repair and maintenance of industrial components. Flux cored self-shielded wires were initially developed for steel construction purposes on the basis of the following concepts:

- (a) the use of aluminium as deoxidiser and denitrider;
- (b) the use of lithium in order to prevent absorption of atmospheric nitrogen from the arc using the principle of thermal diffusion; and
- (c) the use of slag systems containing aluminium and magnesium which desulfurise the weld metal, reducing susceptibility to sulphide hot cracking.

Self-shielded flux cored wires are being used extensively for weld hardfacing to repair and maintain key engineering components that are subjected to damage by wear. The design of these wires is based on the concepts of second and third generations of self-shielded alloy designs, together with additions of the major alloying elements of carbon, chromium and molybdenum.

The effect of the residual Al content on weld metal microstructure has been examined using thermodynamic modeling and dilatometric analysis [3, 4]. It was concluded that the typical residual Al content of about 1 wt% promotes δ -ferrite formation at the expense of austenite and its martensitic/bainitic product phase, thereby compromising the wear resistance of the hardfacing deposit.

The main objective of the present work was to explain structural evolution in the weld metal for a selected alloy design and variable cooling rates after weld deposition.

2 Experimental materials and methods

The chemical composition and classification of the weld deposit are summarized in Tables 1 and 2. As per AS/NZ 2576 specification [6], four test pieces were welded, each with a different pre-heat temperature (100, 200, 300 and 420 °C). Pre-heat temperatures were selected on the basis of standard applicable pre-heat temperatures (100–300 °C), as well as a pre-heat of 420 °C which was higher than the M_S temperatures measured in samples from deposits produced using the specified pre-heats. In order to achieve undiluted weld metal deposits, five layers were welded using the parameters shown in Table 3.

The solidification time, cooling rates and cooling times between 800 and 500 °C were estimated based on the heat input and pre-heat temperature (Table 4).

Table 4 indicates that for pre-heating to 100, 200 and 300 °C, Δt_{8-5} is respectively 7.1, 10.7 and 18.4 s. For the highest pre-heat temperature 420 °C, Δt_{8-5} was much higher at 46 s [8].

Dilatometry was used to simulate the weld thermal cycle experienced by as solidified weld metal subjected to heating by a subsequent weld pass to a temperature of 1100 °C to produce grain refined heat affected zone (GRHAZ) and to 1350 °C to produce the grain coarsened heat affected zone (GCHAZ). Samples for dilatometry were machined from the

as-welded regions of the deposit and were heated at a high rate (50 °C/s) to the peak temperature and held for 2 s before cooling. The imposed cooling rate was linear and was continued to room temperature. The selected cooling rates and the corresponding values of Δt_{8-5} (in parentheses) were as follows: 100 °C/s (3 s), 50 °C/s (6 s), 25 °C/s (12 s), 5 °C/s (60 s) and 1 °C/s (300 s). Therefore, except for the extreme rates of 100 and 1 °C/s, the selected cooling rates correspond approximately to those given in Table 4 for cooling of the actual weld over the 800 to 500 °C temperature range. Although the dilatometric cooling profile (linear) in the high temperature range did not correspond to that of the actual welds (exponential), it was assumed that because of rapid diffusion at elevated temperatures the proportions of ferrite and austenite existing prior to the austenite transformation range for a given pre-heat would be similar for both the dilatometric heat treatment and that of the actual weld. Welds were cross-sectioned and etched with 2.5% Nital for macro- and micro-examination. Cylindrical dilatometer samples were also cross-sectioned for structural examination and hardness testing.

3 Results and discussion

3.1 Macro and microstructures

Microstructural examination of as-deposited weld metals pre-heated up to 300 °C indicated that the structure was dominated by martensite and/or bainite, but contained some residual δ -ferrite. A similar structure was also present for a pre-heat of 420 °C despite the slow cooling rate of 6.5 °C/s ($\Delta t_{8-5} = 46$ s).

The multi-layer welds deposits for pre-heats of 100–300 °C were characterized by three distinct macrostructural regions (Fig. 1): as-deposited (primary) structure, (Region 1); and a heat affected zone (HAZ) that consisted of two main sub-zones—a lighter etching region adjacent to the fusion boundary (Region 2) and a darker etching region (Region 3). The approximate temperature contours relevant to these regions are indicated in Fig. 2 and are discussed in the next section. The origin of this darker etching region was also examined.

The 420 °C pre-heat produced a different result in terms of the macrostructure. The dark etching subzone was effectively absent and the hardness was more uniform throughout the deposit. Despite the average hardness being slightly lower than the maximum values found for lower pre-heats, it was

Table 1 Chemical composition (in wt%) of all-weld metal weld deposit

	%C	%Mn	%Si	%Cr	%Mo	%Al	CE IIW
Alloy B; 1440-B7	0.19	1.37	0.63	2.44	0.56	1.97	1.006
Fe-M1 IIW-II-E-464-04 [5]							

Table 2 Cross reference to International Standards Classification [6]

IIW-II-E-464-04 microstructure type	EN14700 alloy group	DIN 8555 alloy group	JIS Z 3251 and Z 3326 alloy	AS/NZS 2576 alloy	AWS A5.13 and A5.21 alloy group
Fe-M1	1.1, 1.2	1, 2	F2B	14	Fe3, Fe5

concluded [5] that the more uniform hardness associated with the use of a high pre-heat is an advantage in terms of resistance to metal-to-metal adhesive wear.

Despite the different macroscopic regions of the weld deposits, the microstructure throughout the weld deposits consisted a plate- or lath-shaped product phase (tempered martensite and/or bainite) and pockets of δ -ferrite. The current paper addresses the structural evolution as a function of weld pre-heat temperature in an attempt to explain the effect of cooling rate on microstructure and the more uniform hardness when the pre-heat temperature exceeded the M_S temperature.

3.2 Effect of weld metal composition on phase equilibria

Since Al is a strong austenite loop former, solute Al contents above 1 wt% in SSAW weld metal can severely constrict or eliminate the single austenite phase field and thereby compromise the potential for hardening by transformation of austenite to martensite or bainite on cooling. Vertical sections of the phase diagram have been calculated using MT Data for varying C content at selected Al contents [3, 4] and the concentrations of the other elements as recorded in Table 1. These calculated vertical sections showed that the austenite phase field is eliminated for more than 1.5 wt% Al [3, 4] for an alloy with the concentrations of the other elements given in Table 1. Moreover, it was established that a completely austenitic structure can be obtained (i.e. δ -ferrite can be eliminated) for an Al content less than 0.5 wt% [4].

The bulk composition of the deposited alloy (Table 1) indicates a high Al content of 1.18%. As well as Al, the elements Si, Mo and Cr are also austenite loop formers (ferrite stabilizers). For the Fe-Al binary system, the austenite phase field is eliminated for 0.95 wt% Al [9]. The corresponding values for Si, Mo and Cr in their respective binary systems with Fe are 1.9, 2.2 and 12.7 wt% [9]. Therefore, Al is the strongest ferrite former of this group of elements and using the relative “strengths” of the ferrite forming elements, an Al equivalent

can be defined as wt% Al + 0.50 wt% Mo + 0.43 wt% Si + 0.075 wt% Cr [3].

Energy dispersive spectroscopy (EDS) in a scanning electron microscope (SEM) indicated that the solute Al content was lower than the bulk figure of 1.18% (Table 1). A concentration of 0.9 wt% Al was determined for regions of transformed austenite and 1.3 wt% for δ -ferrite. For a typical volume fraction of δ -ferrite of about 0.25, the average solute Al content for the alloy is therefore about 1%. Using this value and the concentrations of Si, Mo and Cr given in Table 1, the Al equivalent of the alloy is about 1.71 wt%. Although an alloy with such a high Al equivalent would be expected to strongly inhibit austenite formation, the strong ferrite forming tendency will be opposed by the presence of the austenite stabilizers: C and Mn, with C having the stronger effect.

The calculated vertical section of the phase diagram for 1 wt% Al (Fig. 2) indicates that cooling of the alloy from the molten state should result in the formation austenite plus δ -ferrite, without the formation of a single austenite phase field. Therefore, although the presence of austenite at elevated temperature will allow the formation of martensite or bainite on relatively fast cooling, some residual δ -ferrite is to be expected.

The alloy investigated does not have a conventional Ae_3 temperature (equilibrium temperature at which 100% austenite is formed), as δ -ferrite is present on heating up to the solidus temperature, T_s , of 1680 K (1407 °C). Therefore, there is no Ac_3 temperature associated with continuous heating. There are however, Ae_1 and Ac_1 temperatures, which correspond to the start of austenite formation on heating of the ferrite-carbide structure present at low temperatures. The phase diagram predicts that the Ae_1 temperature is about 1100 K (827 °C) and the temperature of complete dissolution of carbide (elimination of any tempered martensite or bainite), defined here as Ae_{MC} , is about 1180 K (907 °C) for a very slow heating rate. The corresponding Ac_{MC} temperature will be significantly higher because of the relatively slow kinetics of carbide dissolution. As a consequence, carbide is likely to

Table 3 Welding parameters

Wire size (mm)	Electrode polarity	Volts	Amps	Arc travel speed (mm/min)	Electrical stick out (mm)	Heat input (kJ/mm)
2.8	DC+	28	340	430	70	1.064

Table 4 Estimated thermal cycles for samples welded with different pre-heats. The cooling rate is the average rate between 800 and 500 °C; and Δt_{8-5} is the cooling time between 800 and 500 °C

Pre-heat (°C)	Solidification time (s)*	Δt_{8-5} (s)*	Ave cooling rate (°C/s) from 800–500 °C*
100	1.36	7.1	42.2
200	1.58	10.7	28.0
300	1.85	18.4	16.3
420	2.36	46.0	6.5

*Ref. [7]

persist even after all of the transformable ferrite has reverted to austenite.

The HAZ region (Fig. 1) lies between between T_S and Ac_1 and was found to comprise about 22% of the area of the multi-pass weld zone.

3.3 Dilatometry

Dilatometry was used to simulate the weld metal HAZ generated by heating from a subsequent weld pass to a temperature characteristic of the GRHAZ (1100 °C) and the GCHAZ (1350 °C). The dilatometer simulation results correspond to the region of the actual weld deposit that lies between T_S and Ac_{MC} and is defined as Region 2 in Fig. 1. Samples of the alloy weld metal were heated at a high rate (50 °C/s) to the peak temperature and were held for 2 s before cooling at relatively rapid rates. Therefore, phase evolution is expected to be significantly different from that indicated by the equilibrium phase fields. The first indication of austenite formation (Ac_1) on heating occurred at about 1173 K (900 °C) with a slight flattening of the thermal expansion curve due to the volume contraction associated with transformation of ferrite to austenite, Fig. 3. On heating above 900 °C at 50 °C/s, the volume fraction of austenite increases, as shown by the

upward curvature of the dilatometry curve towards a gradient at elevated temperatures which is close to that expected for a substantially austenitic structure, Fig. 3. Carbide also progressively dissolves on continuous heating, eliminating the vestiges of the tempered martensitic/bainitic structure. The Ac_{MC} temperature at 50 °C/s can be roughly estimated from the dilatometer curve as the termination of the “flattening” plateau associated with significant austenite formation. This temperature is about 1000 °C. The transition temperatures defined by dilatometry have been used to identify the limits of the HAZ regions shown schematically in Fig. 1.

Although tie lines cannot be assumed to lie in the section of multi-component phase diagrams, it was assumed for the present alloy that the maximum weight fraction of austenite occurs at about 1400 K (1137 °C) and that as temperature increases towards the solidus temperature progressive reversion of austenite to δ -ferrite occurs. The dilatometry also indicates that continuous adjustment in the proportions of δ and γ occurs during heating and cooling at rates consistent with the thermal cycle typical of arc welding. However, the changes will lag considerably behind those expected under equilibrium conditions, with the extent of the lag increasing with increasing cooling rate. Moreover, on fast heating the temperature associated with the maximum weight fraction of austenite will be displaced to a higher temperature than that indicated by the equilibrium diagram (1400 K/1127 °C). The maximum austenite fraction formed on heating is likely to lie between the two peak temperatures chosen for simulation (1100 and 1350 °C), and to be closer to the higher peak temperature. Assuming that 100 °C superheat would be required to reach the maximum austenite content on heating at 50 °C/s, the maximum would occur at about 1227 °C, halfway between the two selected peak temperatures.

Returning to Fig. 1, and considering the dilatometer data and the predicted phase equilibria, the width of the lighter etching Region 2 of the actual weld HAZ is considered to be bounded by T_S (1427 °C) and Ac_{MC} (1000 °C), with the darker etching Region 3 extending into the intercritical heat affected zone (ICHAZ) and primary structure that has been

Fig. 1 Schematic diagram of two weld layers and macrograph of actual multi-layer deposit showing three distinct regions of the weld beads. Temperatures at the indicated HAZ boundaries shown on the schematic diagram have been estimated by dilatometry (see text)

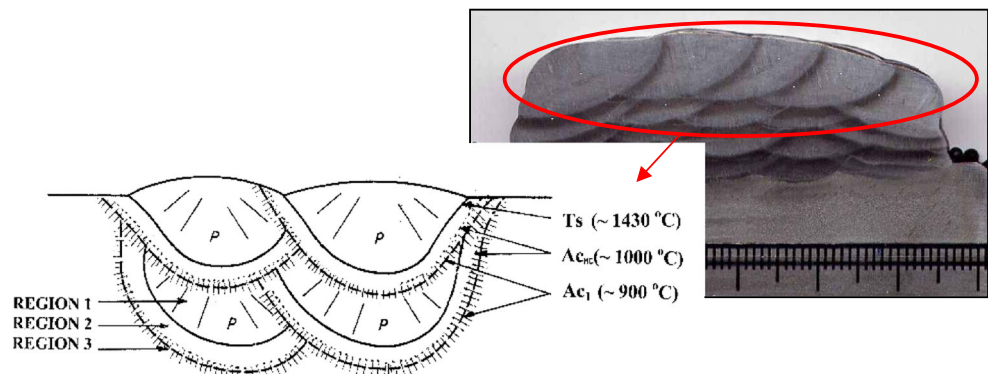
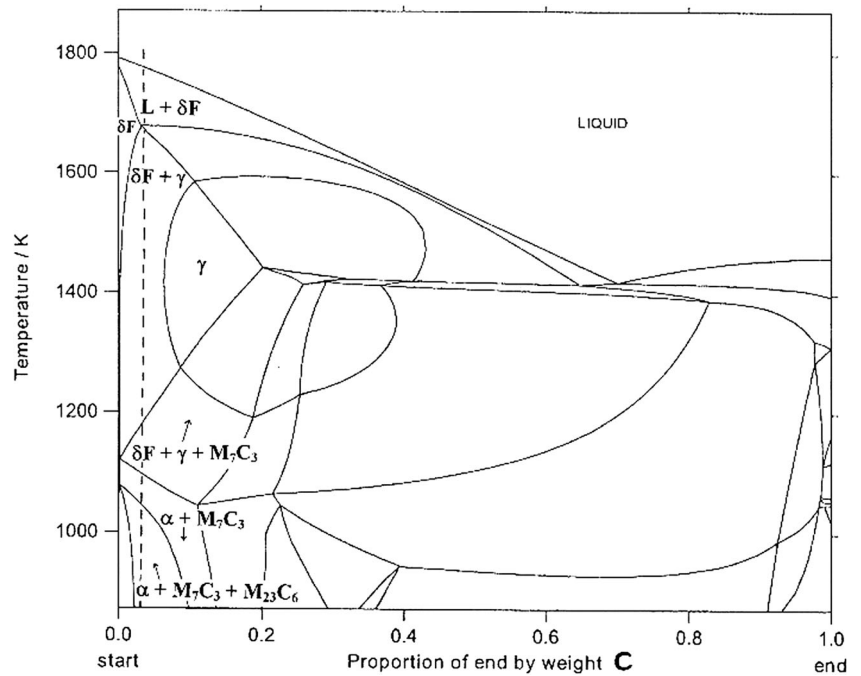


Fig. 2 Vertical section of the phase diagram for the alloy given in Table 1, except for a different Al content (1 wt%) and variable C content. Each 0.2 increment along the x-axis corresponds to 1.2 wt% C. The dashed line represents the alloy C content of 0.18 wt%. Only the phase fields relevant to this composition are identified. (After refs. [3, 4])



reheated to a temperature above about 600 °C. These regions are characterized by the presence of carbide in a matrix of well-tempered martensite/bainite, because they have been exposed to elevated temperatures by subsequent weld passes and to a sustained period at the pre-heat/interpass temperature. In contrast, the adjacent higher temperature region of the HAZ reverted to the maximum amount of austenite and subsequently transformed on cooling to martensite/bainite, which is at a much earlier stage of carbide precipitation (tempering). Therefore, it is inferred that the higher density of carbide/ferrite interfacial area causes Region 3 to respond more strongly to etching.

On cooling at relatively slow rates (1, 5 or 25 °C/s) from the peak temperature progressive reversion to ferrite occurred, resulting in a curved dilatometric trace. However, below about 900 °C, the curve was nearly linear, indicating that there was little or no adjustment to the proportions of δ-ferrite and austenite before the onset of austenite transformation to martensite below 400 °C. For the higher cooling rates of 50 and 100 °C/s, there was less transformation to ferrite during cooling. The effect of cooling rate on the percentage of δ-ferrite retained at ambient is shown in Fig. 4 for the two peak temperatures.

Fig. 3 Dilatometer curves for a simulated weld thermal cycle consisting of heating at 50 °C/s to 1350 °C, holding for 2 s, followed by cooling at 25 °C/s. The small dip in the heating curve just above 700 °C corresponds to the Curie point transition and the perturbation around 650 °C on cooling is due to a change in the flow rate of the cooling gas. Approximate thermal expansion/contraction curves for austenite (A), martensite (M) and ferrite-carbide (F + C) structures for P91 (9% Cr, 1% Mo) martensitic steel, sourced from reference [10], are shown

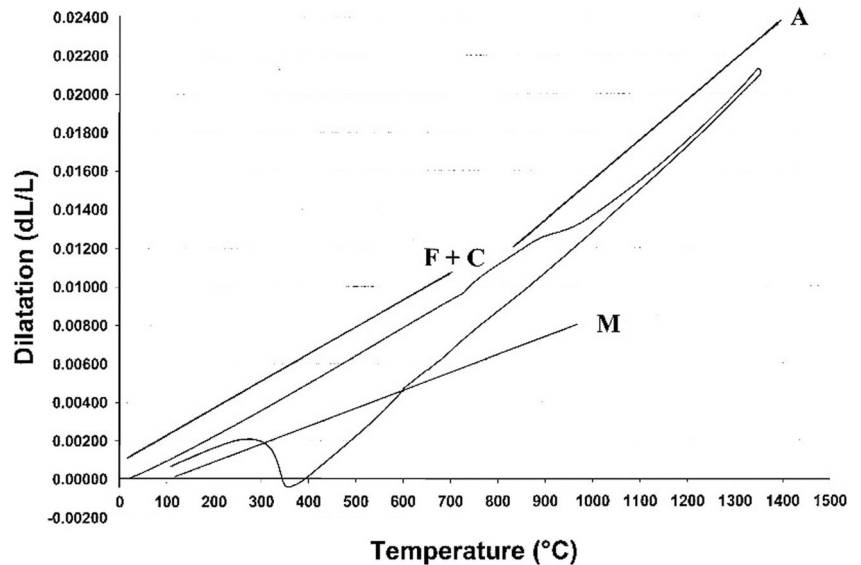
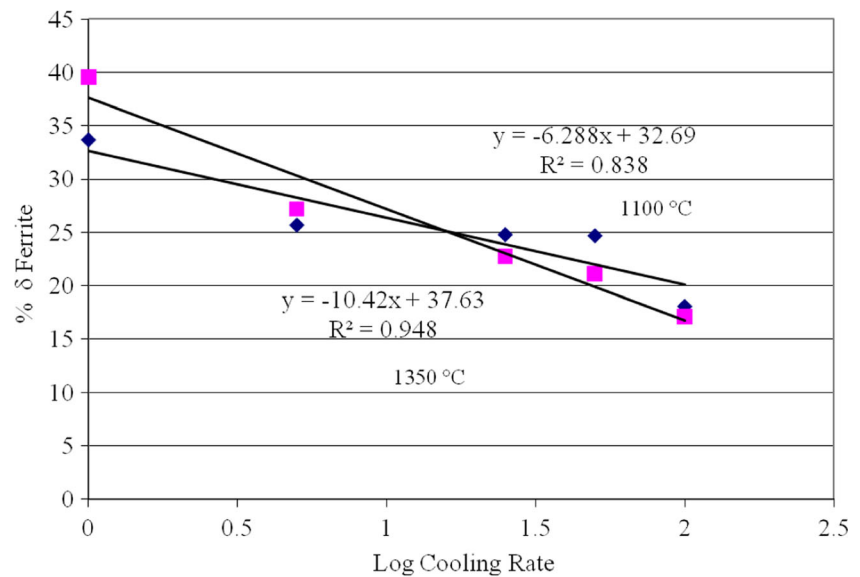


Fig. 4 Percentage of δ -ferrite as a function of the logarithm of cooling rate for simulated weld thermal cycling. Squares are data points for the 1350 °C peak temperature and correspond to the upper linear regression equation. The diamond symbols are for the 1100 °C peak temperature



In general, decreasing the cooling rate resulted in more δ -ferrite, but significantly more δ -ferrite was present for 1350 and 1 °C/s than for 1100 and 1 °C/s. It is inferred that the higher peak temperature allowed more time for reversion of austenite to ferrite on slow cooling. In general, however, the microstructures of the simulated GR and GC HAZs consisted of δ -ferrite distributed in a matrix of martensite (transformed austenite), with the peak temperature and cooling rate influencing the relative proportions of the two phases.

The length change, $\Delta L/L$, associated with martensitic transformation reflects the transformation volume change ($\Delta V/V \sim 3 \Delta L/L$) [11]. The volume change decreased with decreasing cooling rate because the vol. % austenite decreased at the expense of δ -ferrite (Fig. 5). The length difference between martensite and austenite was calculated at a temperature close to M_F using the extrapolated austenite + δ -ferrite contraction curve. This determination is based on comparing the

length of a sample that has just reached M_F on cooling (complete transformation of austenite to martensite) with that of the same sample assumed not to have transformed to martensite at the M_F temperature, (i.e. consisting of δ -ferrite and austenite). The maximum volume change recorded was about 1.6%, corresponding to the transformation of about 80 vol.% austenite at the highest cooling rate of 100 °C/s (Fig. 5). For transformation of an alloy with 100% austenite, the volume change would be expected to be about 2%.

The M_S temperature also increased with increasing cooling rate (Fig. 6). This effect is due decreasing carbon partitioning to austenite on fast cooling and correlates with a decrease in vol.% δ -ferrite (an increase in the vol.% martensite) because of reduced transformation of austenite to δ -ferrite during cooling (Fig. 4).

Babu et al. [12] reported the opposite trend for high Al (1.7 wt%) E70 T-4 weld metal. The volume fraction of δ -

Fig. 5 Percentage volume change as a function of the log. of the cooling rate for simulated weld thermal cycling. Squares are data points for the 1100 °C peak temperature and correspond to the upper linear regression equation. The diamond symbols are for the 1350 °C peak temperature

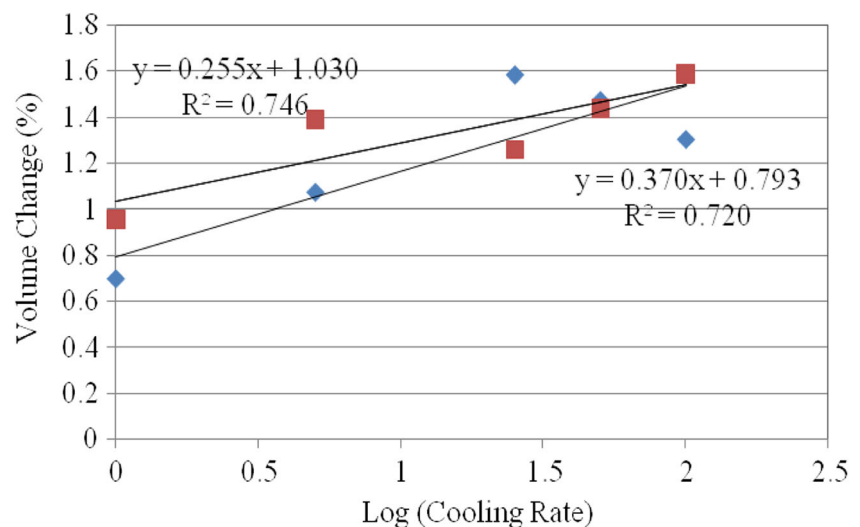
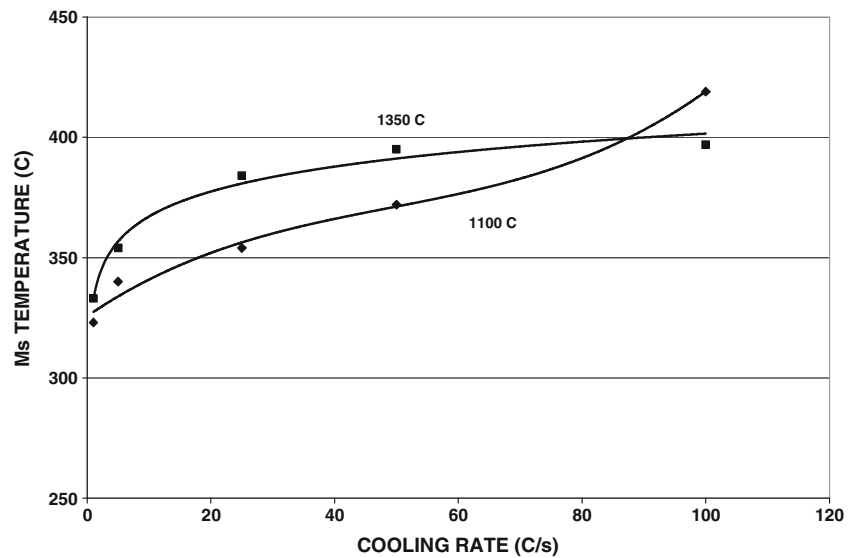


Fig. 6 Effect of cooling rate from the peak temperatures of 1100 and 1350 °C on M_S temperature



ferrite was calculated by computational thermodynamics to be higher at 1600 K (1323 °C) for a cooling rate of 10 K/s compared to 1 K/s. The measured volume fraction of δ -ferrite in the actual weld metal at ambient was about 0.6. Nevertheless, this predicted trend with cooling rate relates to an alloy with a significantly higher Al content than that investigated in the current work. The formation of δ -ferrite at the expense of austenite at high temperatures on re-heating of weld metal in the present case is restricted by the fast heating rate and short dwell time at the peak temperature, resulting in a structure that is dominated by austenite. The extent of reversion to δ -ferrite on subsequent cooling is rate dependent, and was observed to decrease with an increased cooling rate for both the simulated samples and the actual welds.

The relationships between % martensite and average hardness and M_S temperature are shown in Figs. 7 and 8. The trend in hardness correlates well with the increasing volume fraction of martensite (and the corresponding decrease in the relatively soft δ -ferrite phase), dominating a counteractive effect due to the decreasing C content of the martensite. Simultaneous increases in vol.% martensite and M_S occurred with increasing

cooling rate (Figs. 4 and 6, respectively). Therefore, the increases in hardness and M_S with increasing vol.% martensite in Fig. 7 are associated with increasing cooling rate. Figs. 7 and 8 also shows that the peak temperature of the simulated weld thermal cycle had a relatively small effect on hardness and M_S temperature.

The M_S – M_F range was between 120 and 150 °C, consistent with that normally reported [10]. The hardness measurements for the lower peak temperature, simulating the grain refined HAZ, were generally higher, possibly because of a contribution by grain refinement to the alloy hardness.

It should be noted that the austenite decomposition product for all of the cooling rates applied to the dilatometer samples was martensite, confirming the high alloy hardenability that is reflected in the CE (IIW) value (Table 1).

The microstructures of the HAZ of actual weld deposits were similar to those of the dilatometer simulations: δ -ferrite and martensite/bainite. The dilatometer samples were cooled directly to ambient and so the austenite transformed to martensite. It is evident from the dilatometer data (Table 5) that for the actual welds, the 100 and 200 °C pre-heat temperatures are

Fig. 7 M_S temperature of the simulated weld HAZ structures as a function of volume percentage of martensite (circular symbols, 1100 °C; triangular symbols, 1350 °C). The square of the linear correlation coefficient, R , is indicated for each data set.

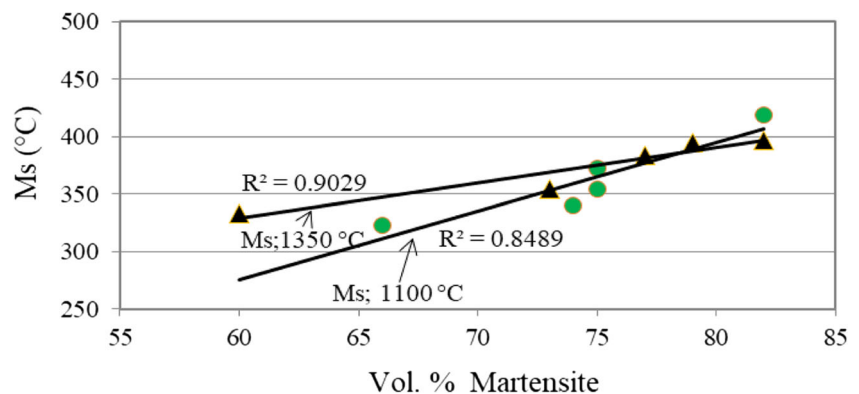
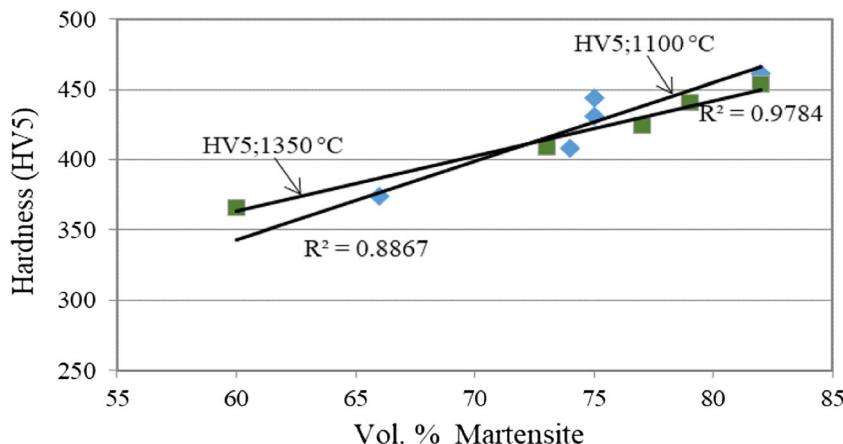


Fig. 8 Vickers hardness of the simulated weld HAZ structures as a function of volume percentage of martensite (diamond symbols, 1100 °C peak temperature; square symbols, 1350 °C). The square of the linear correlation coefficient, R , is indicated for each data set



below M_F . Therefore, the austenite should have transformed completely to martensite. For 300 °C pre-heat, the interpass temperature is below M_S , but not M_F and therefore the structure of the actual welds on isothermal holding at the pre-heat temperature is expected to be a mixture of austenite, martensite and δ -ferrite. Isothermal transformation of austenite to bainite is also possible, with any residual austenite being expected to transform to martensite on subsequent cooling to ambient.

A higher pre-heat temperature (420 °C) was also investigated. This temperature is higher than any of the M_S temperatures reported in Table 5. It is also higher than the M_S prediction of 404 °C reported by Beres et al. [13] for alloy creep resisting steels. However, all empirical equations for M_S assume that the elements are dissolved in a completely austenitic structure before cooling. This assumption is not valid in this case: δ -ferrite is present as well as austenite and at least some of the Al, as intended, is combined with nitrogen and oxygen. As Table 5 and Fig. 4 show, M_S varied markedly with cooling rate, but it was typically lower than the predicted values. Therefore, the primary weld structure during deposition and after cooling to the interpass temperature of 420 °C is likely to be austenite plus columnar regions of residual δ -ferrite, arising from transformation of dendrites of δ -ferrite to austenite by both peritectic and solid state reactions. Primary regions that are reheated to high temperatures below T_S would also be expected to retain a similar structure on cooling to a

temperature of 420 °C or higher. Therefore, if there is no isothermal precipitation of carbide or bainite during subsequent isothermal holding at 420 °C, it follows that the structure throughout the entire weld deposition process would be austenite and δ -ferrite. This assumption was tested by dilatometry and the results are discussed below.

Although the data presented in Figs. 4–8 are based on simulated HAZ treatments that are unlikely to faithfully reproduce the actual thermal cycles occurring in the weld deposit, they are, at least, useful in characterizing the trends in hardness and microstructural evolution of the actual as-welded and HAZ regions of the weld deposit.

3.4 Simulation of isothermal hold cycles

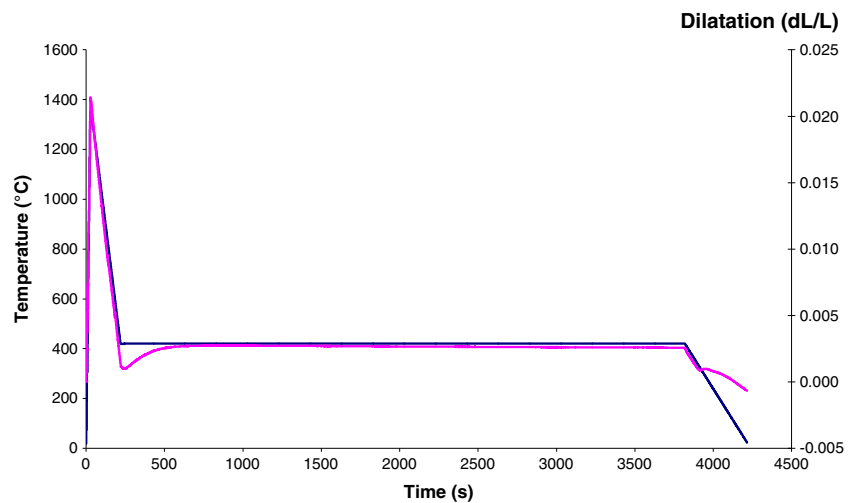
Dilatometer treatments were performed using peak temperatures of 1100 and 1350 °C, a cooling rate of 5 °C/s, and an isothermal hold at 420 °C for 1 h. This cooling rate was selected as it is close to the calculated cooling rate for welds deposited at a pre-heat of 420 °C (6.5 °C/s).

The 1350 °C result is shown in Fig. 9. The specimen dilatation (length change, $\Delta L/L$) was $+1.5 \times 10^{-3}$ (corresponding to a volume change of 0.45%) during the first 500 s at 420 °C, indicating that transformation of austenite occurred isothermally. At the end of the isothermal hold, cooling at 1 °C/s resulted in an additional length increase due to transformation of a small volume fraction of remnant austenite. The M_S

Table 5 Effect of cooling rate on average hardness, vol.% martensite and martensite start (M_S) and finish (M_F) temperatures for samples subjected to simulated thermal cycles

Cooling rate (°C/s)	Peak temperature = 1100 °C				Peak temperature = 1350 °C			
	Hardness (HV5)	Martensite (vol.%)	M_S (°C)	M_F (°C)	Hardness (HV5)	Martensite (vol.%)	M_S (°C)	M_F (°C)
1	374	66	323	205	366	60	333	214
5	408	74	340	210	409	73	354	207
25	431	75	354	224	424	77	384	228
50	444	75	372	221	441	79	395	248
100	461	82	419	238	454	83	397	249

Fig. 9 Temperature and length change as a function of time for a dilatometer sample heated to 1350 °C at 50 °C/s, held for 2 s, then cooled at 5 °C/s to 420 °C and held for 60 min before cooling to ambient at 1 °C/s



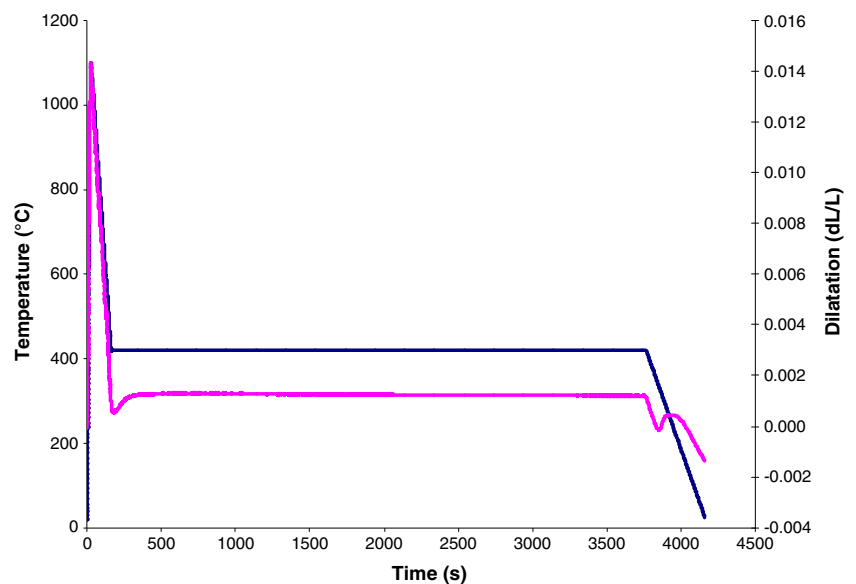
temperature was approximately 324 °C, whereas the measured M_S for direct cooling at 5 °C/s to ambient was 354 °C (Table 5). Figure 9 indicates that in order to induce further transformation after isothermal holding, it was necessary to undercool by nearly 100 °C below 420 °C and 30 °C below the M_S measured for the continuously cooled sample. This observation is similar to that of the well documented phenomenon of austenite stabilization after an arrest within the M_S – M_F range [12]. This stabilization effect is probably due to reduced effectiveness of dislocation nucleation sites for martensite formation caused by formation of C atmospheres, as well as partitioning of C to remaining austenite and associated depression of M_S .

For the 1100 °C peak temperature sample, less transformation of austenite occurred at 420 °C and substantially more martensite formed during cooling after completion of the isothermal hold, Fig. 10. M_S and M_F were about 350 and 180 °C. The measured M_S for a cooling rate of 5 °C/s without an

isothermal hold was actually lower (340 °C). Therefore, it is inferred that the isothermal hold in this case catalysed subsequent transformation to martensite, rather than stabilizing the austenite. A possible explanation is that the relatively small amount of isothermal decomposition of austenite was sufficient to generate a significant number of dislocations in austenite, because of the volume change, to promote martensite nucleation on resumed cooling, despite a counteractive effect due to C segregation to dislocations and C partitioning. The latter effects could be restricted because of relatively large diffusion distances in the substantial volumes of retained austenite.

The origin of the different responses to isothermal holding of the 1100 and 1350 °C samples remains to be explained. Although both samples contained an average of about 75% untransformed austenite when the isothermal arrest temperature of 420 °C was reached, there was microstructural evidence of compositional segregation in the deposits. It is

Fig. 10 Temperature and length change as a function of time for a dilatometer sample heated to 1100 °C at 50 °C/s, held for 2 s then cooled at 5 °C/s to 420 °C and held for 60 min before cooling to ambient at 1 °C/s



therefore possible that the observed difference in isothermal behavior is due to compositional differences between the samples.

Nevertheless, these results indicate that a significant amount of the austenite present on reaching 420 °C transforms isothermally. Since 420 °C is well above the M_S temperatures measured for continuous cooling to ambient (340 °C for the 1100 °C peak temperature and 354 °C for 1350 °C), the decomposition product is likely to be bainite. The observed incompleteness of transformation is also consistent with bainitic transformation [14]. The high Al and Si contents are likely to inhibit precipitation of carbide in company with the formation of bainitic ferrite plates; and to enhance partitioning of C to the remaining austenite [14]. Although the formation of a high volume fraction of bainite may promote stabilization of the small remnant amount of untransformed austenite by enhanced carbon partitioning, the smaller amount of bainite formed for the 1100 °C sample could actually promote nucleation of martensite on subsequent cooling because C partitioning has a relatively more limited effect, as discussed above. Further, compositional segregation in the weld deposit, as also noted above, could result in dilatometer samples with variations in local compositions and therefore, different isothermal and anisothermal transformation characteristics.

The 5 °C/s cooling rate for the simulated samples (Table 5) corresponds approximately to that calculated for a 420 °C pre-heat for the actual weld deposit over the 800–500 °C range (6.5 °C/s, Table 4). The measured average hardness for these simulated samples was 408 HV (1100 °C) and 409 HV (1350 °C). The hardness of the simulated samples, held isothermally at 420 °C, were little different, 393 HV (1100 °C) and 410 HV (1350 °C), despite exposure to the elevated pre-heat temperature for 1 h before linear cooling to room temperature. This apparent anomaly can be explained by the two-stage transformation of the samples. Although the isothermal decomposition product can, in principle, undergo tempering during holding, the high Si content could inhibit formation of carbide in the bainite [14]. Although the martensite that forms on renewed cooling would be essentially untempered, the temperature of its formation would be only slightly lower than that of the bainite, so that the dislocation densities of the two phases would be expected to be similar. The product would remain therefore essentially untempered and have an average hardness similar to that obtained for continuous cooling and transformation in the absence of an isothermal hold.

3.5 Actual weld deposits

The effect of the pre-heat temperature on the structure and hardness of the primary and heat affected regions of the actual weld deposits (Fig. 1) was also investigated. The hardness results are given in Table 6 and a plot of hardness versus pre-heat is shown in Fig. 11. The weld metal (Region 1) showed a

Table 6 Vickers hardness test results (HV 10) for primary (as-deposited) and heat affected regions of the actual welds

		Reg. 1	Reg. 2	Reg. 3
Pre-heat 100 °C	Aver.	423	386	344
Cool rate 42.2 °C/s	Max.	446	409	357
	Min.	413	370	333
	S. Dev.	11	12	6
Pre-heat 200 °C	Aver.	414	361	343
Cool rate 28.0 °C/s	Max.	437	373	357
	Min.	383	342	327
	S.Dev.	13	12	10
Pre-heat 300 °C	Aver.	404	367	341
Cool rate 16.3 °C/s	Max.	437	375	360
	Min.	380	357	322
	S.Dev.	16	8	13
Pre-heat 420 °C 6.5 °C/s	Aver.	390	387	–

decrease in hardness from 423 to 390 HV with increasing pre-heat. Increasing pre-heat has the effect of increasing the proportion of δ -ferrite in both Regions 1 and 2, as well as promoting tempering of the martensitic structure. Despite any retardation of carbide precipitation due to Si, the presence of the strong carbide formers, Cr and Mo, will ensure that carbide formation does occur, particularly because of the applied pre-heat and the prolonged exposure of deposited weld beads to thermal gradients induced by deposition of successive weld beads. The microstructures will trend towards those indicated by the phase diagram shown in Fig. 2. The as-deposited weld metal (Region 1) exhibited hardness values well in excess of those measured in the weld HAZ, Regions 2 and 3, which was subjected to at least partial re-austenitisation.

The higher hardness values for the 100 °C pre-heat correspond to the highest cooling rate and the highest vol.% martensite in Region 2 (Fig. 4). Region 3 has the lowest hardness (about 340 HV10), but the high pre-heat of 420 °C resulted in a rise in hardness in Regions 2 and 3 because of the different modes of austenite transformation (isothermal transformation to bainite and anisothermal transformation to untempered martensite on cooling); and possible secondary hardening in Region 3 due to formation of coherent/semi-coherent alloy carbides. The overall result was a more uniform hardness across the weld metal.

3.6 Comparison of simulated and actual HAZ structures

The average hardness values measured for the re-austenitised Region 2 of the actual welds were lower than the values for the simulated Region 2 samples reported in Table 6 and plotted in Fig. 11, even though the cooling rates of 5, 25, and 50 °C/s for the dilatometer simulations are similar to the calculated rates

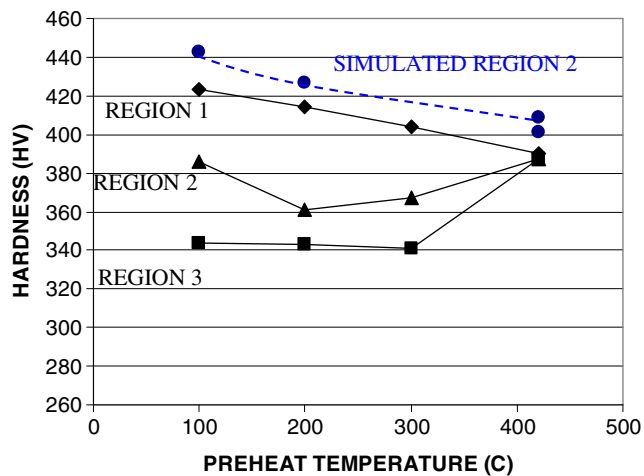


Fig. 11 Hardness as a function of pre-heat temperature for the three regions of the actual weld defined in Fig. 1. Diamond symbols—Region 1; triangles—Region 2; and squares—Region 3. The upper points (circles) correspond to average hardness values for the simulated samples cooled at rates close to those corresponding to pre-heat temperatures of 100, 200 and 420 °C, with two hardness values for 420 °C: the upper one corresponding to continuous cooling and the lower to isothermal holding

of 6.5, 28 and 42 °C/s, corresponding to the actual welds for pre-heats of 420, 200 and 100 °C. The average hardness (HV10) for re-austenitised regions of the actual welds was 387, 361 and 386 for pre-heats of 420, 200, and 100 °C, respectively. The corresponding average hardness values for the simulated samples were 409, 428 and 443 HV. The cooling rate for the weld deposit produced with a pre-heat of 200 °C (28 °C/s) is close to the 25 °C/s cooling rate used for one of the dilatometer simulations. However, the average hardness of the lighter etching HAZ region, T_S – A_{CMC} , of the actual weld was 361 HV, compared to 431 HV for the simulated weld thermal cycle with a peak temperature of 1100 °C and 424 HV for the peak of 1350 °C. Therefore, Region 2 of the actual weld was softer than the simulated Region 2 samples by more than

about 50 HV points. The reason for this difference is clearly the absence of any pre-heat for the dilatometer treatments. The exposure of the transformed re-austenitised regions to the elevated pre-heat temperature during the deposition process resulted in significant tempering of the martensite, particularly for the 300 °C pre-heat. In addition, the cooling time below 500 °C is more relevant than Δt_{8-5} in relation to auto-tempering of transformation product formed above the pre-heat/interpass temperature, and is considerably longer for the actual welds.

The dilatometry conducted with a 420 °C isothermal hold for 60 min. Obviously provided a more accurate simulation of the actual weld thermal cycle for the case of the 420 °C pre-heat. The hardness values for the simulated 420 °C hold samples were 393 HV (1100 °C) and 410 HV (1350 °C), an average of 402 HV, whereas the average hardness of the HAZ region, T_S – A_{CMC} , in the actual weld was 387 HV10 (see Table 6 and Fig. 11). The slightly lower average hardness measured for the actual weld could arise from fluctuations above 420 °C due to temperature control problems during the multi-pass weld deposition process and the effect of the slow exponential fall to ambient after welding, as opposed to linear 1 °C/s cooling rate for the simulated thermal cycle.

The origin of the “dark etching” Region 3 has been alluded to previously. In effect, regions that are exposed to elevated temperatures and retain at least some undissolved and coarsened carbide (~600–1000 °C) will be substantially tempered, leading to the dark etching response and reduced hardness (Table 6). In contrast, reheating of as solidified weld metal to temperatures above about 1000 °C should result in substantial re-austenisation at the expense of ferrite. The austenite grains become equi-axed and on cooling transform to martensite and/or bainite. Although pre-heat/interpass temperatures up to 300 °C will serve to temper these freshly transformed regions, precipitation will be retarded relative to regions of the as-welded structure that are exposed to high

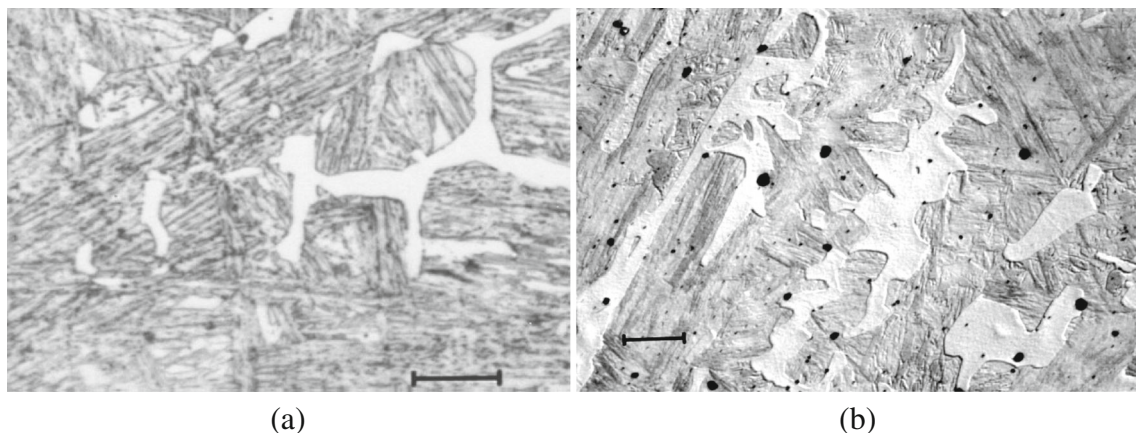
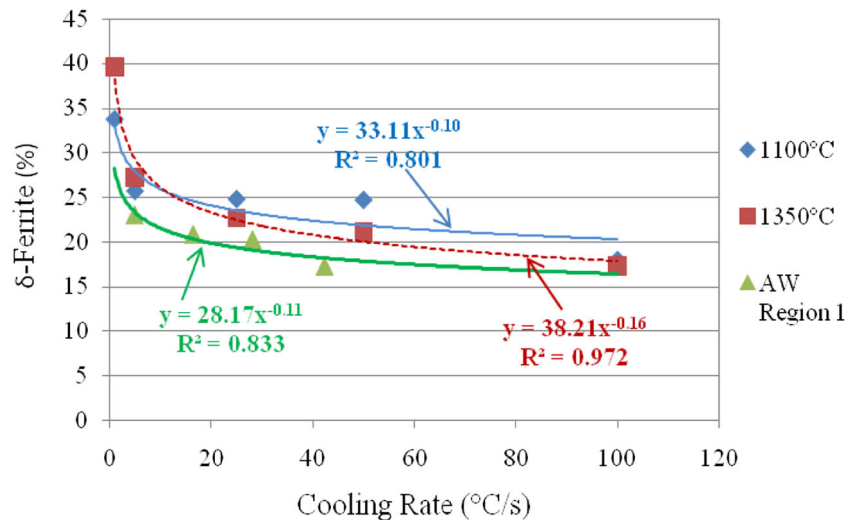


Fig. 12 Microstructures of the actual weld deposit (a); and a dilatometer sample subjected to a simulated weld thermal cycle to 1350 °C peak temperature, followed by cooling at 25 °C s⁻¹ (b). The bars represent 20 μm

Fig. 13 Volume % of δ -ferrite as a function of cooling rate of dilatometry samples heated to maximum temperatures of 1100 and 1350 °C and Region 1 of the as-welded (AW) samples. Square symbols correspond to the 1350 °C peak temperature; diamond symbols correspond to the 1100 °C peak temperature; and triangles represent as-welded Region 1



temperatures, short of those required for complete austenitisation (less than ~ 1000 °C). The “dark” etching response of these regions implies the presence of a high density of carbides whose interfaces with the ferrite matrix are grooved by the etchant, resulting in significant scattering of incident light and therefore, a reduction in the intensity of reflected light that is intercepted by the eye. The “light” etching HAZ region is due to a higher reflected light intensity because the precipitation of carbide in “freshly” formed martensite/bainite is more limited.

The disappearance of the “dark etching” region for the 420 °C treatment is due to the etch contrast effect becoming less obvious. Although the microstructure across the multi-pass weld deposit would still be expected to be heterogeneous, this high pre-heat treatment acts like an in-process postweld heat treatment, which serves the function of reducing hardness gradients across the weld deposit, as well as across the parent plate HAZ, that arise from substructural factors such as differences in dislocation density and state of precipitation. Figure 11 shows that despite the marked decrease in the average hardness of the as-welded microstructure with increasing pre-heat temperature, the hardness of the HAZ region rises sufficiently to produce greater weldment homogeneity in terms of hardness. It is inferred that the other mechanical properties, including wear resistance, will be enhanced relative to those of weldments produced using conventional and lower pre-heats. Further, the high pre-heat treatment would be expected to provide more effective relief of residual stresses.

Microstructures of Regions 1 and 2 of the actual weld metal deposits, as well as those of simulated GR and GC HAZs, consisted of δ -ferrite distributed in a matrix of martensite (transformed austenite). Examples of the as-welded Region 1 microstructure and the simulated Region 2 microstructure are given in Fig. 12. Although compositional segregation and microstructural heterogeneity in the weld deposit caused local variability in the proportions of δ -ferrite and martensite,

extensive quantitative measurements of volume fraction of δ -ferrite in the actual weld and the simulated HAZ structures established the consistent trends with cooling rate shown in Fig. 13.

The relationships between cooling rate and percentage of δ -ferrite (Fig. 13) indicate close agreement of the results for dilatometry and the actual welds. The correlation coefficients are relatively high, indicating that the equations derived for each case provide a good fit of the data. The overall mutual consistency of the results confirms that the volume% δ -ferrite is sensitive to the cooling rate during welding (Fig. 13).

4 Conclusions

Structural evolution and the hardness of a high aluminium SSAW hardfacing deposit have been rationalized in terms of phase equilibria and kinetics of phase transformation. The presence of a substantial amount of Al in the flux composition is designed to protect the molten metal from gas porosity arising from absorbed oxygen and nitrogen. However, a consequence of excess solute Al in the weld metal of the alloy investigated is that a fully austenitic alloy cannot be obtained at high temperature (i.e. there is no A_{c3} temperature) and therefore full transformation hardening is not possible.

Decreasing the cooling rate of dilatometer samples subjected to simulated weld thermal cycles resulted in decreases in vol.% martensite, the magnitude of the transformation volume change and the M_s temperature. These trends are consistent with a decreasing volume fraction of austenite with an increasing C content as the cooling rate decreases. Therefore, this investigation has established that the weld thermal cycle can profoundly alter the volume fraction and carbon content of the martensite that forms on cooling. Strong differences were observed in the contrast of distinct regions of the macrostructure of actual welds deposited at pre-heats of 100, 200 and 300 °C.

These differences can be explained on the basis of variation in the state of tempering of the major regions of the deposit, which affects the local etching response and imparts contrast in the macro- and microstructures of the weld metal. Pre-heating to 420 °C eliminated this contrast effect because of more uniform tempering of the whole weld deposit. This pre-heat temperature was above M_S and thermal simulations established that partial transformation of austenite to bainite occurred during isothermal holding with remnant austenite transforming to martensite on subsequent cooling to ambient. Despite the multiphase microstructure of δ -ferrite, bainite and martensite, the high pre-heat temperature provides a normalising heat treatment that reduces differences in dislocation density and carbide precipitation across the various weld regions and results in a considerably more uniform weldment hardness than that of the deposits produced with the lower, more conventional, pre-heats.

References

- Kotecki DJ (1992) Hardfacing benefits- maintenance and repair. *Weld J* 71(11):51–53
- Kotecki GJ, Osborn JS (1995) Abrasion resistance of iron-based hardfacing alloys. *Weld J N Y* 74(8):269–278
- Dumovic M, Dunne D (2014) Prediction of weld metal microstructure of self-shielded arc hardfacing welds resistant to metal-to-metal wear. *Weld World* 58(6):831–837
- Dumovic M, Monaghan BJ, Li H, Dunne D (2015) Weld metal microstructures of hardfacing deposits produced by self-shielded flux-cored arc welding. *Australas Weld J Weld Res Suppl* 60(1st Qtr):40–48
- Dumovic M, Norrish J, Dunne D (2008) Effect of pre-heat on properties of low carbon martensitic steel weld overlays for adhesive metal-to-metal wear resistance, international conference: “Safety and reliability of welded components in energy and processing industry”, 61st IIW annual assembly, Graz Austria
- Australian and New Zealand Standard (2005) Welding consumables for build-up and wear resistance, AS/NZS 2576, Standards Australia; International Institute of Welding 2004, A Classification System for Hardfacing Alloys, IIW-II-1545-04
- Chob LT, Chin MT (1995) Heat flow in fusion welding, ASM handbook, vol 6, Welding, Brazing and Soldering, 7–19
- Adams CM Jr (1958) Cooling rate and peak temperatures in fusion welding. *Am Weld Soc Weld J* 37:210–215
- ASM Metals Handbook (1973) vol. 8, 8th edn. Metallography, structures and phase diagrams
- Sulaiman S (2007) Structure and properties of the heat affected zone of P91 creep resistant steel, PhD Thesis, University of Wollongong, NSW, Australia
- Christian JW (1970) In: Petty ER (ed) Martensite—fundamentals and technology, Chapter 3—Basic Crystallography and Kinetics. Longman Group Limited, Harlow, UK, pp 36–41
- Babu SS, David SA, Quintana MA (2001) Modeling microstructure development in self-shielded flux cored arc welds. *Weld J*:91–97s
- Beres L, Imer W, Balogh A (1997) *Sci. Tech. Weld Join* 2(5):236–238
- Bhadeshia HKDH (1992) Bainite in steels. The Institute of Materials, London